Structural Engineering and Mechanics, Vol. 10, No. 1 (2000) 37-51
DOI: http://dx.doi.org/10.12989/sem.2000.10.1.037

Results and implications of the damage index method applied to a multi-span continuous segmental prestressed concrete bridge

Ming L. Wang†, Fan L. Xu‡ and George M. Lloyd‡†

Department of Civil and Material Engineering, University of Illinois at Chicago, 842 West Taylor Street 2095 ERF, Chicago, IL. 60607, U.S.A.

Abstract. Identification of damage location based on modal measurement is an important problem in structural health monitoring. The damage index method that attempts to evaluate the changes in modal strain energy distribution has been found to be effective under certain circumstances. In this paper two damage index methods using bending strain energy and shear strain energy have been evaluated for numerous cases at different locations and degrees of damage. The objective is to evaluate the feasibility of the damage index method to localize the damage on large span concrete bridge. Finite element models were used as the test structures. Finally this method was used to predict the damage location in an actual structure, using the results of a modal survey from a large concrete bridge.

Key words: strain energy; damage index method; concrete bridge.

1. Introduction

This paper deals with the problem of using changes in the mode shapes of structures to nondestructively detect and locate the damage using the damage index method. In addition to the commonly used damage index based upon bending strain energy, a new index method based upon shear strain energy is proposed and compared with the former. Both damage index methods using bending strain energy and shear strain energy have been evaluated for numerous cases at different locations and degrees of damage. The objective of this paper is to evaluate the feasibility of the damage index method to localize the damage. Finite element models were used as the test structures. Finally this method was used to predict the damage location in an actual structure, using the results of a modal survey from a large concrete bridge.

This paper is organized as follows. We first derive the damage index method based upon strain energy originally proposed by Kim and Stubbs (1995, 1996). Second, formulas for the two damage index methods are derived on the assumption that bending and shear strain energy can be separated. Then the two methods are analyzed using the results of a finite element simulation of a large span pre-stressed segmental concrete bridge (Satpathi, Chen, Wang and Kim 1999, Wang, Xu, Satpathi and Chen 1999). Finally, the results from the implementation of the two algorithms on the measured

† Professor
‡ Ph.D. Student
‡† Postdoctoral Associate

mode shapes are given.

2. Theoretical description of damage index method

Consider a linear, elastic and undamaged structure with NE elements and N modes. The ith modal strain energy of the structure is given by

$$U_i=\Phi_i^T K\Phi_i \tag{1}$$

Φ_i represents the ith mode shape vector and K is the system stiffness matrix. Since the structure is linear, the jth member contribution of the ith modal strain energy, U_{ij}, is given by

$$U_{ij}=\Phi_i^T K_j\Phi_i \tag{2}$$

K_j is the contribution of jth member to the system stiffness matrix. For the ith mode, the fraction of the modal strain energy of total structure and the jth member, (which is also called the modal sensitivity for the ith mode in jth location) is given by

$$F_{ij}=U_{ij}/U_i \tag{3}$$

For the damaged structure, the modal sensitivity for the ith mode in jth location is defined in a similar way,

$$F_{ij}^*=U_{ij}^*/U_i^* \tag{4}$$

where

$$U_i^*=\Phi_i^{*T} K^*\Phi_i^* \tag{5}$$

$$U_{ij}^*=\Phi_i^{*T} K_k^*\Phi_i^* \tag{6}$$

Asterisks denote quantities associated with a damaged structure. K_j and K_j^* in Eq. (2) and Eq. (5) may be separated into a material part and a geometry part as follows:

$$K_j=E_jC_{j0} \tag{7}$$

$$K_j^*=E_j^*C_{j0} \tag{8}$$

E_j and E_j^* are parameters representing material properties (for example, the Young's modulus). The matrix C_{j0} involves only geometric quantities (and possibly terms containing Poisson's ratio). For a given mode i, the modal sensitivities in Eq. (3) and Eq. (4) have the following properties

$$\sum_{j=1}^{NE} F_{ij}^*=\sum_{j=1}^{NE} F_{ij}=1 \tag{9}$$

If it is assumed that the structure is discretized into a large number of small elements, it is reasonable to assume that no single elemental modal sensitivity dominates. This can be written as follows:

$$F_{ij}<<1,\quad F_{ij}^*<<1 \tag{10}$$

The most important assumption is now made that the modal sensitivities for the ith mode at the jth location is the same for both undamaged and damaged structure, yielding the following relation

$$F_{ij}=F_{ij}^{*} \tag{11}$$

Substituting Eqs. (3) and (4) into Eq. (11) yields,

$$1=\frac{F_{ij}^{*}}{F_{ij}}=\frac{U_{ij}^{*}/U_{i}^{*}}{U_{ij}/U_{i}} \tag{12}$$

Substituting Eqs. (1), (2), (5) and (6) into Eq. (12) and rearranging, the damage index, β_{ij}, which is related to the change in the modal strain energy stored in member j for ith mode, is written as

$$\beta_{ij}=\frac{E_j}{E_j^{*}}=\frac{\gamma_{ij}^{*}U_i}{\gamma_{ij}U_i^{*}} \tag{13}$$

In this expressions, $\gamma_{ij}=\Phi_i C_{j0}\Phi_i$ and $\gamma^{*}_{ij}=\Phi_i^{*}C_{j0}\Phi_i^{*}$.

For N measured modes, the damage index, β_j, which represents the change in the modal strain energy stored in the member j for N modes, is written as

$$\beta_j=\frac{E_j}{E_j^{*}}=\frac{\sum_{i=1}^{N}\gamma_{ij}^{*}U_i}{\sum_{i=1}^{N}\gamma_{ij}U_i^{*}} \tag{14}$$

If the element size is very small and the elements are located at nodes of a vibrational mode simultaneously, the denominator in Eq. (12) will be zero. To avoid potential numerical problems, unity was added to both the numerator and denominator of Eq. (12) and yields

$$1=\frac{F_{ij}^{*}+1}{F_{ij}+1}=\frac{(U_{ij}^{*}+U_i^{*})U_i}{(U_{ij}+U_i)U_i^{*}} \tag{15}$$

Although there does not seem to be a rigorous foundation for this procedure, it has been used with reported success (Kim and Stubbs 1995, Stubbs and Kim 1996).

If this development is accepted, and Eqs. (1), (2), (5), and (6) are substituted into Eq. (15), it gives damage index, β_{ij}, as follows:

$$\beta_{ij}=\frac{E_j'}{E_j^{*}}=\frac{(\gamma_{ij}^{*}+\sum_{k=1}^{NE}\gamma_{ik}^{*})U_i}{(\gamma_{ij}+\sum_{k=1}^{NE}\gamma_{ik})U_i^{*}} \tag{16}$$

For N measured modes, the damage index, β_j, is written as

$$\beta_j=\frac{E_j}{E_j^{*}}=\frac{\sum_{i=1}^{N}\left[\left(\gamma_{ij}^{*}+\sum_{k=1}^{NE}\gamma_{ik}^{*}\right)U_i\right]}{\sum_{i=1}^{N}\left[\left(\gamma_{ij}+\sum_{k=1}^{NE}\gamma_{ik}\right)U_i^{*}\right]} \tag{17}$$

If the structure is considered as an elastic beam, the strain energy can be written in the following way

$$U=U_{shear}+U_{bending}=\sum_{i=1}^{NE}\frac{1}{2}\int_{x_i}^{x_i+\Delta x_i}\left[\frac{GA}{\kappa}\left(\frac{dw}{dx}-\theta\right)^2+EI\left(\frac{d\theta}{dx}\right)^2\right]dx \tag{18}$$

It is assumed in a linear theory that the total deflection can be related to an effect due to bending and an effect due to shear, where w is the transverse displacement and θ is the rotation of section. For a thin beam ($A_c<<L_c^2$), the shear strain is negligible. This implies that $\theta=\theta_b$ and $w=\theta_b$, yielding

$$\frac{dw}{dx}-\theta\approx 0 \tag{19}$$

With this assumption, Eq. (18) can be simplified to the following

$$U=\sum_{i=1}^{NE}\frac{1}{2}\int_{x_i}^{x_i+\Delta x_i}\left[EI\left(\frac{d\theta}{dx}\right)^2\right]dx \tag{20}$$

So the modal strain energy under the assumption of negligible shear strain can be written as

$$U_{ij}=EI\int_{x_j}^{x_j+\Delta x_j}(\Phi''_{i(x)})^2dx \quad U^*_{ij}=EI^*\int_{x_j}^{x_j+\Delta x_j}(\Phi^{*''}_{i(x)})^2dx \tag{21}$$

And

$$U_i=\int_0^L EI(\Phi''_{i(x)})^2dx \quad U^*_i=\int_0^L EI^*(\Phi^{*''}_{i(x)})^2dx \tag{22}$$

If assumption $EI=EI^*$=Const. in Eq. (22), the Eq. (15) becomes

$$\beta_j=\frac{\sum_{i=1}^{N}\left[\int_{x_j}^{x_j+\Delta x_j}(\Phi^{*''}_{i(x)})^2dx+\int_0^L(\Phi^{*''}_{i(x)})^2dx\right]/\int_0^L(\Phi^{*''}_{i(x)})^2dx}{\sum_{i=1}^{N}\left[\int_{x_j}^{x_j+\Delta x_j}(\Phi''_{i(x)})^2dx+\int_0^L(\Phi''_{i(x)})^2dx\right]/\int_0^L(\Phi''_{i(x)})^2dx} \tag{23}$$

For a deep beam, the shear strain is the main factor and let

$$\frac{d\theta}{dx}\approx 0 \tag{24}$$

Eq. (18) then simplifies to,

$$U=\sum_{i=1}^{NE}\frac{1}{2}\int_{x_i}^{x_i+\Delta x_i}\left[\frac{GA}{\kappa}\left(\frac{dw}{dx}\right)^2\right]dx \tag{25}$$

So the model strain energy can be written as

$$U_{ij}=\frac{GA}{\kappa}\int_{x_j}^{x_j+\Delta x_j}(\Phi'_{i(x)})^2dx \quad U^*_{ij}=\frac{GA^*}{\kappa}\int_{x_j}^{x_j+\Delta x_j}(\Phi^{*'}_{i(x)})^2dx \tag{26}$$

$$U_i=\int_0^L\frac{GA}{\kappa}(\Phi'_{i(x)})^2dx \quad U^*_i=\int_0^L\frac{GA^*}{\kappa}(\Phi^{*'}_{i(x)})^2dx \tag{27}$$

If assumption $GA=GA^*$=Const. in Eq. (27), the Eq. (15) can be written as

$$\beta_j=\frac{\sum_{i=1}^{N}\left[\int_{x_j}^{x_j+\Delta x_j}(\Phi^{*'}_{i(x)})^2dx+\int_0^L(\Phi^{*'}_{i(x)})^2dx\right]/\int_0^L(\Phi^{*'}_{i(x)})^2dx}{\sum_{i=1}^{N}\left[\int_{x_j}^{x_j+\Delta x_j}(\Phi'_{i(x)})^2dx+\int_0^L(\Phi'_{i(x)})^2dx\right]/\int_0^L(\Phi'_{i(x)})^2dx} \tag{28}$$

In order to form a statistic which can discriminate among damaged and undamaged elements, the β_j are assumed to be random variables. A standardized statistic, which has mean zero regardless of the actual distribution of β_j, is the following

$$Z_j=\frac{\beta_j-\bar{\beta}_j}{\sigma_j} \tag{29}$$

where $\bar{\beta}_j$ and σ_j are mean and standard deviation of collection of indicators of β_j respectively.

The decision rule for this is as follows: (1) If $Z<2$, there is no damage. (2) If $Z\geq 2$, there is damage. This criterion corresponds to a one-tailed test at a significance level of 0.023(97.7% confidence level). It should be noted that the basis for this development has not been substantiated and is currently under investigation.

3. Modal analysis of finite element models

The objective here is to evaluate the feasibility of damage index method to localize the damage. The finite element models are used as the test structures. These numerical models simulate the real structure and have the same geometry, material properties and support conditions. But they are set to different states of damage by reducing some elements elastic modulus. The real bridge is situated four miles south of Rockford, Illinois. It carries four lanes of the I-39, a major north-south highway, over the Kishwaukee River. There are two identical parallel bridges, with each bridge carrying two lanes of traffic. Each bridge is composed of 5 continuous spans (Fig. 1).

The bridge is a continuous single-cell box girder constructed with precast concrete segments which are then post-tensioned together. Each segment has a top width of 41 ft and a constant depth of 11 ft 4 in. Overall dimensions of a typical midspan segment are given in Fig. 2.

The eigenvalue analysis was performed using ABAQUS. This code can simulate both material and geometrical nonlinearities. The entire bridge is modeled using 1480 shell elements (deck of the bridge), 1184 solid elements (webs and bottom slab of the bridge), and 26788 reinforced rebar elements to simulate prestressing bars (distributed in the bridge).

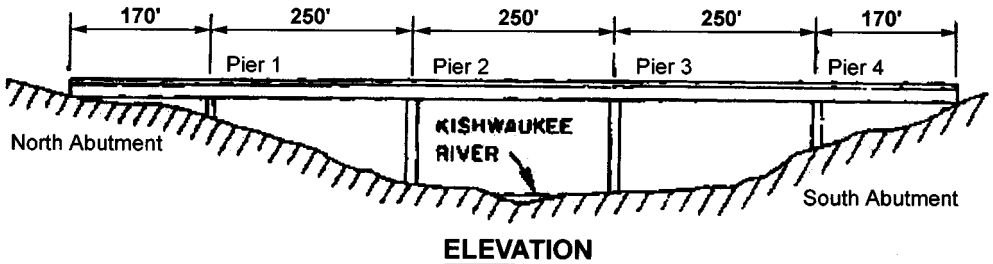

Fig. 1 Longitudinal layout of Kishwaukee Bridge

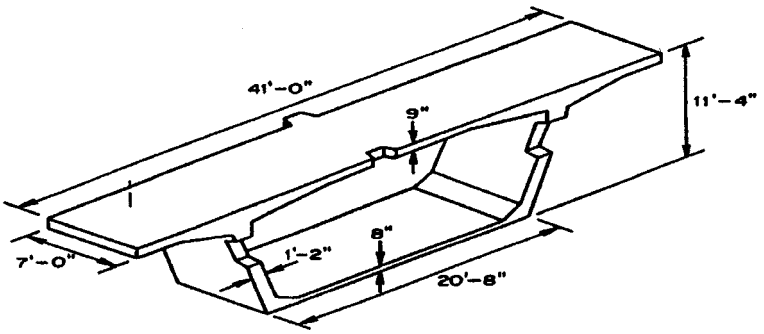

Fig. 2 Dimension of a typical midspan segment

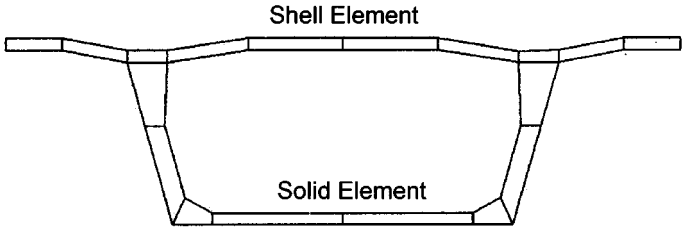

Fig. 3 Cross-section of the developed Finite Element model of the structure

Fig. 3 shows the cross section of the model. The deck of the bridge is modeled as shell elements with continuously varying thickness, and the rest of the section is simulated as three-dimensional solid elements (eight nodes). There are eight solid elements and ten shell elements in one segment. Multiple prestressed cables were incorporated according to the original design drawings. The type of boundary condition was specified as close as possible to the practical situation. The abutment location was pinned while the piers were fixed only in vertical and lateral directions. The material properties are as follows: 1) The Young's modulus E=2.896e10(Pa) (webs and bottom slabs) and E=2.969e10(Pa) (decks) 2); Poisson's ratio γ=0.333; 3) The mass density ρ=2.65e3(kg/m^3); 4) The tendon stress σ=9.377e8(Pa). Total bridge was divided into 148 segments as shown in Fig. 4.

Fig. 5 gives the first three mode shapes for a typical damage case. In view of Eq. (21), Fig. 5 indicates that, qualitatively, modal strain energy is concentrated toward the middle spans of the bridge.

4. Field dynamic modal testing

Visual inspection of the structure reveals the presence of a large number of cracks on the structure in the interior of the box girder. Most of the cracks have originated at the web shear key which is

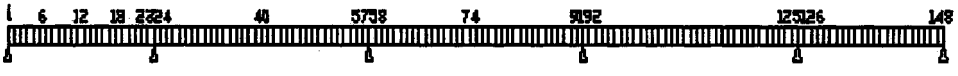

Fig. 4. Finite element model in longitudinal

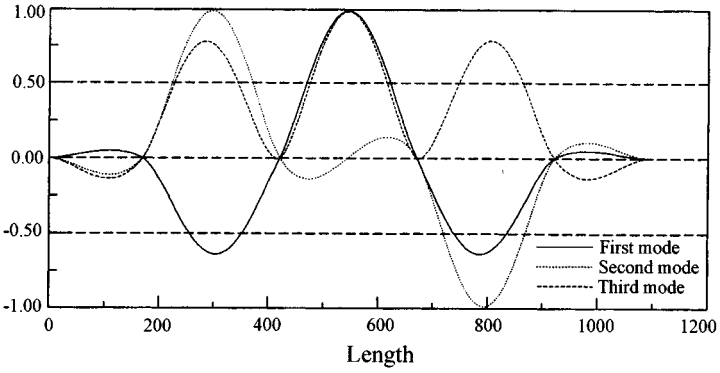

Fig. 5 First three mode shapes for typical damage case

shown in Fig. 2. A typical mapping of the crack pattern on one of the southbound span is shown in Fig. 6. The pier segments that are provided with prestressed diaphragms have very few cracks.

Two sets of measurements were made for the field modal test: 1) ambient vibration from existing traffic flow, and 2) forced vibration using a transient excitation from a Swedish drop hammer. The response of the bridge under normal traffic loading was measured. The measurements were taken only when heavy trucks passed over the bridge to ensure sufficient signal strength and signal duration.

The instrumentation for these series of measurements consisted of 18 piezoelectric accelerometers (Dytran 3187b1, normal sensitivity--1V/g, resolution–10g, usable frequency range–0.53–KHz) and a 32 channel dynamic data acquisition and analyzer system (Zonic corp., model PC7000). The data acquisition system was controlled by proprietary software Zeta, and the data analysis was carried out in MeScope (Vibration Technology Inc.). The comparison of mode shapes obtained by finite element simulation and field measured are shown in Fig. 7. These comparisons are qualitative in the sense that they do not provide a specific description of the location or the magnitude of model

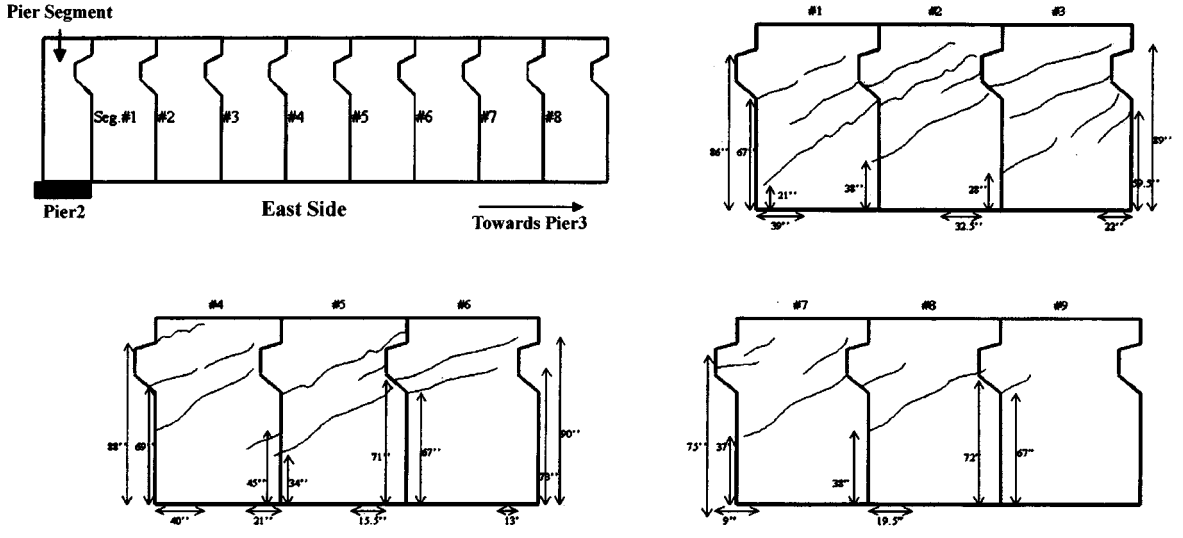

Fig. 6 Crack pattern observed on the inside east web of the southbound bridge

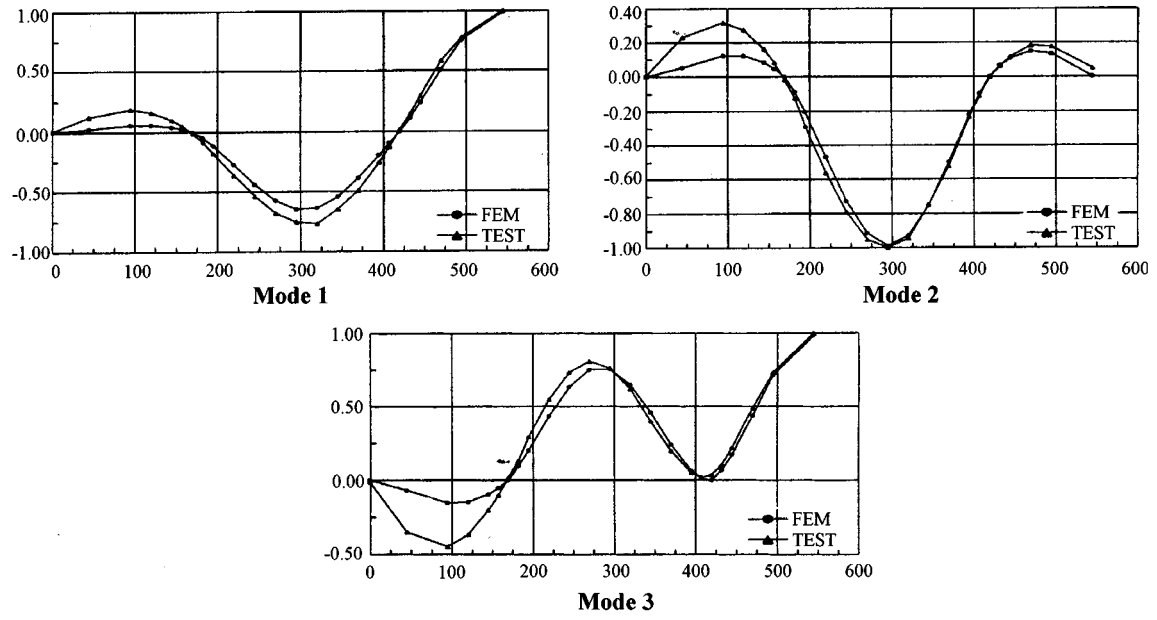

Fig. 7 Comparison of mode shapes between measured and computed results for half bridge

elements or support conditions which may differ between the bridge and the mode. However, they show a systematically large modal deflection in the first span of the real bridge. Further details are given in reference 6.

5. Damage localization for finite element simulation and field measurement

The damage of the simulated structure was defined by altering the material properties from the calibrated model properties. In here, if one segment was damaged, the Young's modulus of the segment, which includes eight solid elements and ten shell elements, was reduced simultaneously. Different damage cases were considered and were divided into four groups. In first and fourth group, the damage was limited to one place and the severity of damage is 10%, 20%, 30%, 40%, and 50%. (Severity=$((E-E^*)/E)\times 100\%$). In the second group there are multiple damaged locations and the severity is 10% and 50%. In the first, second and fourth groups, each damage location only has one damaged segment. In the third group, there are more than eight damage locations and each location has five damage segments. The severity of damage is 10%, 30% and 50%. These multiple damage scenarios were examined since preliminary work suggested a complex dependence of sensitivity of the damage index method to damage location.

Two extreme cases were considered. One considers only the bending strain energy and Eq. (23) was used to predict the damage location. This case was used in the first, second and third groups. The other only considers the shear strain energy and Eq. (28) was used to localize the damage location in the fourth group. The damage scenarios, natural frequencies and damage prediction results are shown in Tables 1-4. The typical normalized damage localization indicator for four groups is shown in Figs. 8-11 (The diagram in the lower part of the plot shows the bridge and its supports).

Table 1 The damage scenarios, natural frequencies and damage prediction results (group one)

Damage case	Natural frequency (Hz)			Simulated damage		Predicted damage	
	First	Second	Third	Location	Severity*	location	VDLI**
1	1.8064	2.0153	2.3276	1	10	none	---
2	1.8063	2.0151	2.3272	1	20	none	---
3	1.8062	2.0147	2.3268	1	30	none	---
4	1.8061	2.0143	2.3262	1	40	none	---
5	1.8060	2.0140	2.3258	1	50	none	---
6	1.8064	2.0155	2.3278	6	10	none	---
7	1.8064	2.0154	2.3276	6	20	none	---
8	1.8063	2.0152	2.3275	6	30	none	---
9	1.8063	2.0150	2.3272	6	40	none	---
10	1.8062	2.0148	2.3269	6	50	none	---
11	1.8064	2.0154	2.3277	12	10	none	---
12	1.8063	2.0152	2.3275	12	20	none	---
13	1.8063	2.0150	2.3272	12	30	none	---
14	1.8062	2.0147	2.3268	12	40	none	---
15	1.8061	2.0144	2.3263	12	50	none	---
16	1.8064	2.0154	2.3277	18	10	none	---
17	1.8063	2.0151	2.3274	18	20	none	---
18	1.8062	2.0148	2.3269	18	30	none	---
19	1.8061	2.0143	2.3264	18	40	18	5.8
20	1.8059	2.0136	2.3254	18	50	18	7
21	1.8062	2.0150	2.3274	23	10	23	6.2
22	1.8059	2.0144	2.3269	23	20	23	9.5
23	1.8056	2.0136	2.3263	23	30	23	11.4
24	1.8053	2.0126	2.3256	23	40	23	13
25	1.8048	2.0114	2.3246	23	50	23	13.2
26	1.8055	2.0135	2.3267	40	10	40	7
27	1.8042	2.0110	2.3252	40	20	40	10.2
28	1.8027	2.0079	2.3234	40	30	40	9.8
29	1.8006	2.004	2.3212	40	40	40	10.1
30	1.7976	1.9987	2.3184	40	50	40	9.8
31	1.8057	2.0132	2.3239	57	10	57	10.8
32	1.8048	2.0103	2.3192	57	20	57	12
33	1.8037	2.0066	2.3136	57	30	57	12.2
34	1.8023	2.0018	2.3066	57	40	57	12.3
35	1.8006	1.9953	2.2978	57	50	57	12.8
36	1.8041	2.0155	2.3259	74	10	74	8
37	1.8012	2.0155	2.3235	74	20	74	9.7
38	1.7976	2.0155	2.3206	74	30	74	9.5
39	1.7928	2.0155	2.3169	74	40	74	9.9
40	1.7863	2.0154	2.3121	74	50	74	10.1

Severity=((E-E*)/E)×100%
VDLI–Value of damage location indicator

Table 2 The damage scenarios, natural frequencies and damage prediction results (group two)

Damage case	Natural frequency (Hz)			Simulated damage		Predicted damage	
	First	Second	Third	Location	Severity[1]	location	VDLI[2]
1	1.8062	2.0149	2.3273	12, 23	10	None	---
2	1.8045	2.0103	2.3232	12, 23	50	23	13
3	1.8052	2.0130	2.3262	23, 40	10	None	---
4	1.7955	1.9947	2.3155	23, 40	50	23, 40	5,9
5	1.8047	2.0112	2.3228	40, 57	10	40, 57	4, 10
6	1.7906	1.9784	2.2907	40, 57	50	40, 57	4.8, 11
7	1.8033	2.0132	2.3219	57, 74	10	57, 74	9.4, 4.3
8	1.7811	1.9950	2.2817	57, 74	50	57, 74	11, 5
9	1.8045	2.0119	2.3261	23, 24	10	23, 24	12, 12
10	1.7887	1.9879	2.3151	23, 24	50	23, 24	14, 14
11	1.8033	2.0124	2.3199	57,58	10	57, 58	13, 13
12	1.7807	1.9868	2.2697	57,58	50	57, 58	14.5, 14.5
13	1.8052	2.0128	2.3261	12,23,40	10	23, 24	3.8, 8
14	1.7951	1.9935	2.3142	12,23,40	50	23, 24	4.8, 9
15	1.8045	2.0106	2.3223	23,40,57	10	23, 40, 57	2, 4.8, 9.8
16	1.7882	1.9741	2.2882	23,40,57	50	23, 40,57	2.2, 4.8, 10.9
17	1.8021	2.0106	2.3203	23,40,57,74	10	23,40,57,74	2,4.8,8.8,3.8
18	1.7698	1.9731	2.2717	23,40,57,74	50	23,40,57,74	2,4,9.8,4

Severity=((E-E*)/E)×100%
VDLI-Value of damage location indicator

Table 3 The damage scenarios, natural frequencies and damage prediction results (group three)

Damage case	Natural frequency (Hz)			Simulated damage		Predicted damage	
	First	Second	Third	Location	Severity[1]	location	VDLI[2]
1	1.7897	1.9946	2.3030	19-23,24-28,53-57 58-62,87-91,92-96 121-125,126-130	10	24-28,53-57 58-62,87-91,92-96 121-125	3.5,3.0, 3.5,3.5,3.0, 3.5
2	1.7471	1.9313	2.2069	19-23,24-28,53-57 58-62,87-91,92-96 121-125,126-130	30	24-28,53-57 58-62,87-91,92-96 121-125	3.9,3.2 4.0,4.0,3.2 4.0
3	1.6866	1.8456	2.0829	19-23,24-28,53-57 58-62,87-91,92-96 121-125,126-130	50	24-28,53-57 58-62,87-91,92-96 121-125	4.2,3.3 4.0,4.0,3.2 4.2
4	1.7896	1.9940	2.3023	1-5,19-23,24-28 53-57,58-62,87-91 92-96,121-125 126-130,144-148	10	24-28 53-57,58-62,87-91 92-96,121-125	3.2 2.9,3.7,3.7 2.9,3.2
5	1.7467	1.9297	2.2047	1-5,19-23,24-28 53-57,58-62,87-91 92-96,121-125 126-130,144-148	30	24-28 53-57,58-62,87-91 92-96,121-125	4.0 3.3,4.0,4.0 3.3,4.0
6	1.6860	1.8429	2.0792	1-5,19-23,24-28 53-57,58-62,87-91 92-96,121-125 126-130,144-148	50	24-28 53-57,58-62,87-91 92-96,121-125	4.2 3.2,4.0,4.0 3.2,4.2

Severity=((E-E*)/E)×100%
VDLI-Value of damage location indicator

Table 4 The damage scenarios, natural frequencies and damage prediction results (group four)

Damage case	Natural frequency (Hz)			Simulated damage		Predicted damage	
	First	Second	Third	Location	Severity[1]	location	VDLI[2]
1	1.8064	2.0153	2.3276	1	10	none	---
2	1.8063	2.0151	2.3272	1	20	none	---
3	1.8062	2.0147	2.3268	1	30	none	---
4	1.8061	2.0143	2.3262	1	40	none	---
5	1.8060	2.0140	2.3258	1	50	none	---
6	1.8064	2.0155	2.3278	6	10	none	---
7	1.8064	2.0154	2.3276	6	20	none	---
8	1.8063	2.0152	2.3275	6	30	none	---
9	1.8063	2.0150	2.3272	6	40	none	---
10	1.8062	2.0148	2.3269	6	50	none	---
11	1.8064	2.0154	2.3277	12	10	none	---
12	1.8063	2.0152	2.3275	12	20	none	---
13	1.8063	2.0150	2.3272	12	30	none	---
14	1.8062	2.0147	2.3268	12	40	none	---
15	1.8061	2.0144	2.3263	12	50	none	---
16	1.8064	2.0154	2.3277	18	10	none	---
17	1.8063	2.0151	2.3274	18	20	none	---
18	1.8062	2.0148	2.3269	18	30	none	---
19	1.8061	2.0143	2.3264	18	40	none	---
20	1.8059	2.0136	2.3254	18	50	none	---
21	1.8062	2.0150	2.3274	23	10	none	---
22	1.8059	2.0144	2.3269	23	20	23	6.4
23	1.8056	2.0136	2.3263	23	30	23	7
24	1.8053	2.0126	2.3256	23	40	23	7
25	1.8048	2.0114	2.3246	23	50	23	7
26	1.8055	2.0135	2.3267	40	10	40	3.5
27	1.8042	2.0110	2.3252	40	20	40	3.5
28	1.8027	2.0079	2.3234	40	30	40	3.5
29	1.8006	2.004	2.3212	40	40	40	3.5
30	1.7976	1.9987	2.3184	40	50	40	3.5
31	1.8057	2.0132	2.3239	57	10	57	7.8
32	1.8048	2.0103	2.3192	57	20	57	8.1
33	1.8037	2.0066	2.3136	57	30	57	8.1
34	1.8023	2.0018	2.3066	57	40	57	8.1
35	1.8006	1.9953	2.2978	57	50	57	8.1
36	1.8041	2.0155	2.3259	74	10	74	4.2
37	1.8012	2.0155	2.3235	74	20	74	4.0
38	1.7976	2.0155	2.3206	74	30	74	3.5
39	1.7928	2.0155	2.3169	74	40	74	3.5
40	1.7863	2.0154	2.3121	74	50	74	3.5

Severity=((E-E*)/E)×100%
VDLI-Value of damage location indicator

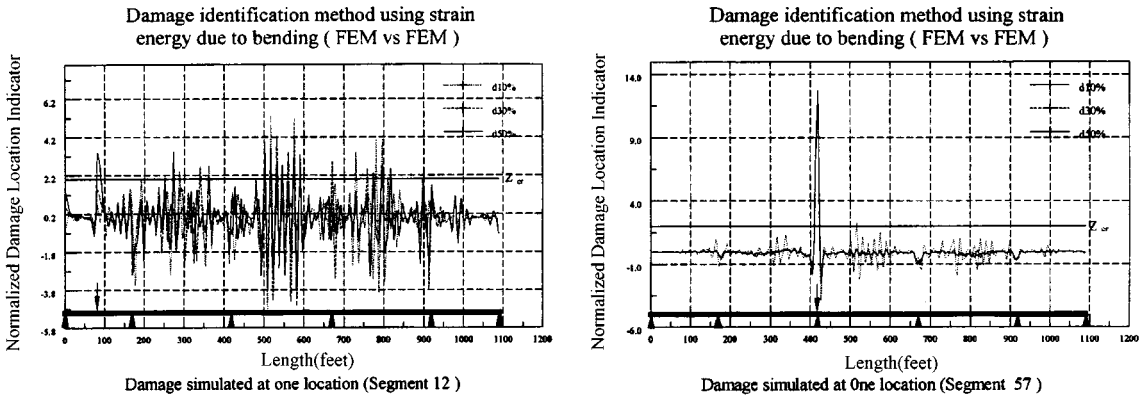

Fig. 8 Normalized damage location indicator using bending strain energy

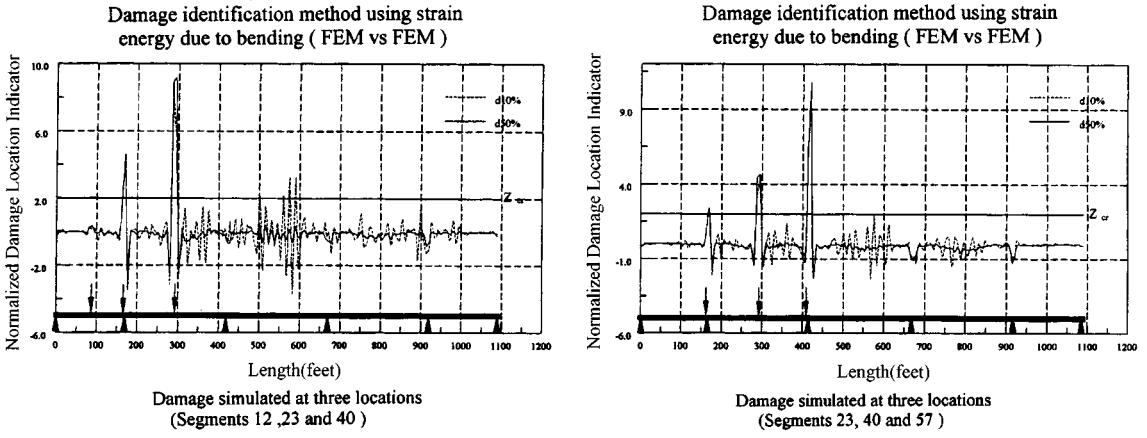

Fig. 9 Normalized damage location indicator using bending strain energy

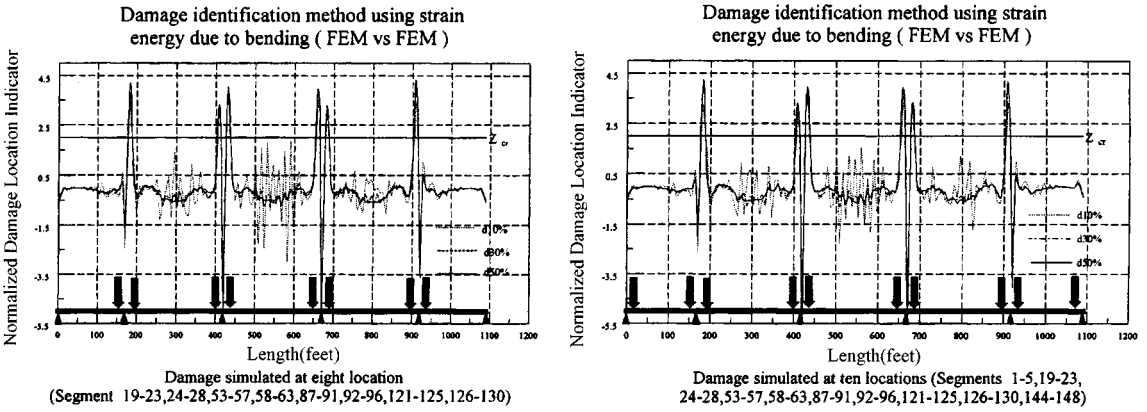

Fig. 10 Normalized damage location indicator using bending strain energy

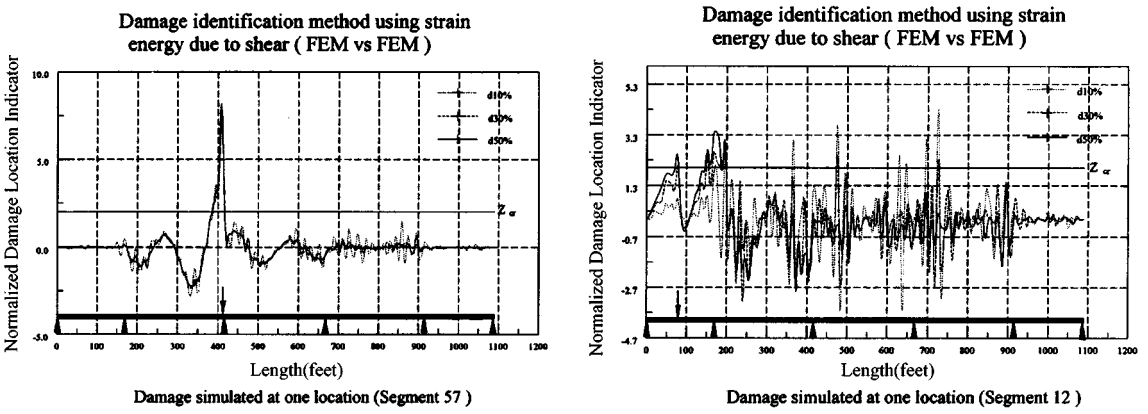

Fig. 11 Normalized damage location indicator using shear strain energy

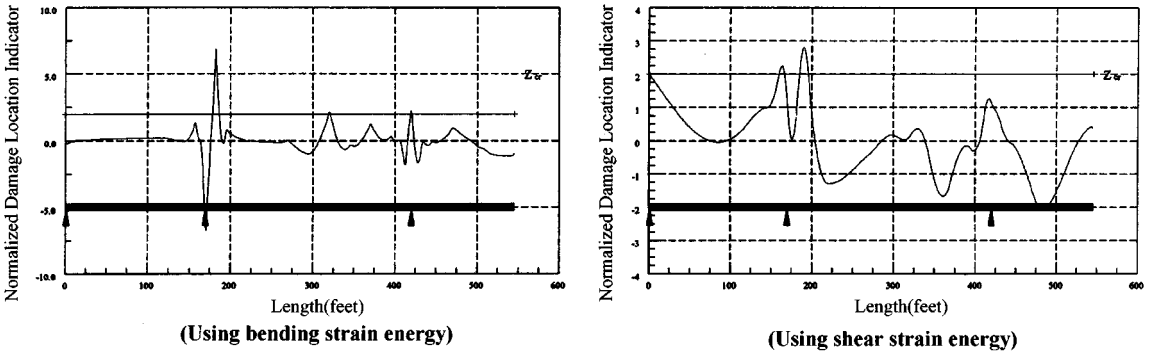

Fig. 12 Damage index method applied to field measurement data

The results which are shown in Figs. 8-11, for damage studied using the FEM-FEM simulations, show in general that the damage index approach clearly identifies the damage location on the basis of the critical value of Z=2.0, provided that the damage location is not in the first span. This is the case for both damage index methods. Additionally, it is evident from the signal to noise ratio of the index magnitude to the critical value of Z that false alarm rates are minimized for damage states greater than 10-20%. These results are in agreement with previous results that show excellent identification for large states of damage (Stubbs, Kim and Farrar 1995, Farrar, Baker and Beu 1994).

Based on the present analysis, it is difficult to correlate the magnitude of the damage index with damage magnitude. As discussed earlier, the "random variable" formulation of the damage index may not be appropriate for all purposes.

The field measurement data also were used for damage identification analysis. Both damage index methods using bending strain energy and shear strain energy have been evaluated for this actual structure. The results from the implementation of that algorithm on the field measured mode shapes are shown in Fig. 12.

The damage index using bending energy shows a peaked response in the vicinity of the first pier support. The results of Fig. 12 must be interpreted with caution for two reasons. First, they presume

a FEM model that has been perfectly calibrated to the existing structure as it had been built. This goal is difficult to achieve in practice, and practically impossible to substantiate for such a large structure as a bridge. Secondly, the FEM-FEM result showed a clear tendency to perform poorly at identifying localized stiffness changes in the first span (see Fig. 8, for example). Quantification of the implications of these comparisons requires further work which addresses the influence of the assumptions employed in the theoretical development for both damage index methods

6. Conclusions

Both damage index methods using bending strain energy and shear strain energy have been evaluated for numerous cases at different locations and degrees of damage. Further analysis of the shear strain DIM results is still required. However, this preliminary analysis of the results leads to the following conclusions. First, without regard to location or damage magnitude, the method correctly located damage states approximately 70% of the time. When the data is analyzed by taking into account location, it is clear that the method is most successful in the center of structure and suffers considerable difficulty near the abutment. Second, these results are based on analyzing the damage index indicator with the traditional assumption that the damage index indicator is a normally distributed random variable. That this is in fact so under the two hypotheses of damage and no damage does not appear to have been investigated before and a proof is lacking. Further theoretical numerical studies are required to justify this assumption. Doing so may lead to a greater effectiveness in capturing damage near the abutment. Third, the studies here show that neither of the damage index methods can estimate the severity of damage. Further work is needed in this area.

References

Catbas, F.N., Brown, D. and Lenett, M. (1997), "Model analysis of multi-reference impact test data for steel stringer bridges", *Proceedings of 15th International Modal Analysis Conference* (Orlando, FL).

Doebling, S.W., Farrar, C.R. and Prime, M.B. (1996), "Damage identification and health monitoring of structural and mechanical systems from changes in their vibration characteristics: A literature review", LA-113070-MS, Los Alamos National Laboratory.

Duffey, T.A., Baker, W.E., Farra, C.R. and Rhee, W.H. (1999), "Detection of damage in axial (Membrane) system", *Proceedings of 17th International Modal Analysis Conference* (Kissimmee, FL), 876-881.

Farrar, C.R., Baker, W.E. and Bell, T.M. (1994), "Dynamic characterization and damage detection in the I-40 Bridge over the Rio Grand", LA-12767-MS, Los Alamos National Laboratory.

Garcia, G.V., Osegueda, R. and Meza, D. (1999), "Damage detection comparison between damage index method and ARMA method", *Proceedings of 17th International Modal Analysis Conference* (Kissimmee, FL), 593-598.

Kim, J.T. and Stubbs, N. (1995), "Model-uncertainty impact and damage-detection accuracy in plate girder", *Journal of Structural Engineering, ASCE*, **121**(10), 1409-1417.

Stubbs, N. and Kim, J.T. (1996), "Damage localization in structures without baseline old parameters", *AIAA Journal*, **34**(8), 1644-1649.

Stubbs, N. Kim, J.T. and Farrar, C.R. (1995), "Field verification of a nondestructive damage location and severity estimation algorithm", *Proceedings of 13th International Modal Analysis Conference*, (Nashville Tennessee) Feb.

Satpathi, D., Chen, Z.L., Wang, M.L. and Kim, J.L. (1999), "Monitoring and modeling of a prestressed segmental box bridge", *Proceedings of SPIE, Smart Structures and Materials*, 1-2 March, **3671**, 257-267.

Wang, M.L., Xu, F.L., Satpathi, D. and Chen, Z.L. (1999), "Modal testing for a multi-spans continuous segment prestressed concrete bridge", *Proceedings of SPIE, Smart Structures and Materials* 1-2 March, **3671**, 328-336.
Wang, M.L., Heo, G. and Satpathi, D. (1998), "A health monitoring system for large structural systems", *Smart Materials and Structures*, 7(5), 606-616.

Notation

U	Strain energy
U_i	ith modal strain energy of undamaged structure
U_{ij}	the jth member contribution of the ith modal strain energy for undamaged structure
Φ_i	ith mode shape vector of undamaged structure
Φ_i^*	ith mode shape vector of damaged structure
K	system stiffness matrix of undamaged structure
K_j	contribution of jth member to the system stiffness matrix of undamaged structure
F_{ij}	modal sensitivity for the ith mode in jth location for undamaged structure
U_i^*	ith modal strain energy of damaged structure
U_{ij}^*	the jth member contribution of the ith modal strain energy for damaged structure
Φ_i^*	ith mode shape vector of damaged structure
K^*	system stiffness matrix of damaged structure
K_j^*	contribution of jth member to the system stiffness matrix of damaged structure
F_{ij}^*	modal sensitivity for the ith mode in jth location for damaged structure
E_j	material properties for undamaged structure
E_j^*	material properties for damaged structure
C_{j0}	geometric matrix of undamaged structure
C_{j0}^*	geometric matrix of damaged structure
β_{ij} β_j	damage index
β	mean of damage index
N	number of mode shapes
NE	number of elements
EI, EI^*	bending stiffness of undamaged and damaged structure
GA, GA^*	shear stiffness of undamaged and damage structure
θ	rotation of section
κ	shear factor
w	transverse displacement